

**Above-barrier fusion enhancement of proton-halo systems**E. F. Aguilera,<sup>\*</sup> P. Amador-Valenzuela, E. Martinez-Quiroz, and J. Fernández-Arnáiz*Departamento de Aceleradores, Instituto Nacional de Investigaciones Nucleares, Apartado Postal 18-1027, Código Postal 11801 México, Distrito Federal, México*

J. J. Kolata

*Physics Department, University of Notre Dame, Notre Dame, Indiana 46556-5670, USA*

V. Guimarães

*Instituto de Física, Universidade de São Paulo, P.O. Box 66318, 05389-970 São Paulo, São Paulo, Brazil*

(Received 22 October 2015; revised manuscript received 19 February 2016; published 16 March 2016)

Previously reported data for fusion of the  ${}^8\text{B} + ({}^{58}\text{Ni}, {}^{28}\text{Si})$  systems are critically reviewed. New  $\alpha$ -particle data from the fusion of  ${}^8\text{B} + {}^{58}\text{Ni}$  also are reported, but the paper is mostly based on using realistic calculations of well-established codes to reanalyze the previous data. The influence of breakup protons on the evaporation proton measurements for the heavier system is found to be small at all energies except for the lowest one measured, and corrections are made for this process. Possible model dependencies in the deduced fusion cross sections are investigated using three different evaporation codes. The data sets for the  ${}^{58}\text{Ni}$  and  ${}^{28}\text{Si}$  targets are shown to be consistent with each other and with fusion enhancement up to energies that are greater than the Coulomb barrier  $V_b$  ( $E_{\text{c.m.}} \lesssim V_b + 1.5 \times \hbar\omega$ ). This limit corresponds to 6.2 MeV above the barrier for the  ${}^{58}\text{Ni}$  target. An important difference with the behavior of neutron-halo systems is thus confirmed.

DOI: [10.1103/PhysRevC.93.034613](https://doi.org/10.1103/PhysRevC.93.034613)**I. INTRODUCTION**

Fusion data for projectiles with a proton-halo ground state are presently quite scarce. The first measurements of this type were for the  ${}^8\text{B} + {}^{58}\text{Ni}$  system [1], for which fusion cross sections ( $\sigma_{\text{fus}}$ ) were reported at ten energies in the near- and sub-barrier region. Later, similar data were published for  ${}^8\text{B} + {}^{28}\text{Si}$  [2] at four energies well above the respective Coulomb barrier. In both experiments, a single type of evaporated charged particle was measured, and fusion cross sections were deduced from the respective experimental yields using statistical-model calculations. In Ref. [1], evaporation protons were measured and fusion cross sections were deduced using the evaporation code PACE2 [3]. The main advantage of this technique results from the fact that the compound nucleus,  ${}^{66}\text{As}$ , is right at the proton-drip line so the corresponding proton multiplicity is high ( $M_p \sim 2.3$ ). In this case, measuring protons is like looking at fusion with a magnifier. This is a highly desirable feature, especially for weak radioactive ion beams. In addition, the results of the statistical-model calculations for  $M_p$  are expected to be more stable for a bigger value of  $M_p$ . One disadvantage is that only an inclusive measurement can be made because protons coming from breakup (bu) of  ${}^8\text{B}$  into  ${}^7\text{Be} + p$  cannot be distinguished from evaporation protons. The low value of the respective threshold energy (0.138 MeV) tends to favor the occurrence of the bu process. Previous CDCC (Continuum Discretized Coupled Channels) calculations [4] indicated that bu protons peak at forward angles, and extrapolation of the published angular distribution to backward angles seemed to indicate

negligible cross section at angles above  $\sim 115^\circ$ . With this available information, the proton detectors in Ref. [1] were placed at backward angles ( $110^\circ$ – $160^\circ$ ) and the contribution of bu protons was neglected. However, on the basis of additional calculations including extended angular distributions (which became available after the publication of Ref. [1]), it was suggested that the bu protons might have had a non-negligible contribution to the data [5].

As for the  ${}^8\text{B} + {}^{28}\text{Si}$  system (Ref. [2]), evaporation  $\alpha$  particles rather than protons were measured and fusion cross sections were deduced using the evaporation code CASCADE (Ref. [6]). The multiplicity issue that was favorable for the  ${}^8\text{B} + {}^{58}\text{Ni}$  system becomes a liability in this case because the respective  $\alpha$ -particle multiplicity is low ( $M_\alpha \sim 0.5$ ). In addition, the corresponding statistical-model calculations are expected to be less stable in this case, which would confer a higher degree of model dependency on the final results for  $\sigma_{\text{fus}}$ . However, the fact that  $\alpha$  particles are unlikely to be products of direct processes with  ${}^8\text{B}$  is a very good asset for this technique.

When plotted together using reduced units (see below), the  $\sigma_{\text{fus}}$  values for the two proton-halo systems seemed to follow quite different trends [2,5]. On the one hand, the  ${}^8\text{B} + {}^{58}\text{Ni}$  system showed fusion enhancement at all measured energies, even above the Coulomb barrier. This contrasts with what has been observed for neutron-halo systems, where total fusion cross sections seem to be suppressed with respect to a standard reference for energies above the barrier [7,8]. This result was unexpected, especially because the total reaction cross sections behave similarly for both neutron-halo and proton-halo systems. Indeed, it has been shown that, after reasonable data reduction, the reduced total reaction cross sections for  ${}^8\text{B} + {}^{58}\text{Ni}$  and for several neutron-halo systems fall on the same trajectory when plotted as a function of the reduced energy [9]. On

<sup>\*</sup>eli.aguilera@inin.gob.mx

the other hand, the  ${}^8\text{B} + {}^{28}\text{Si}$  system seems to present fusion suppression above the barrier [2], which would indicate a similar behavior with respect to neutron-halo systems but an inconsistency with the trend observed for the heavier proton-halo system. However, it should be pointed out that there is little data overlap between measurements of the two systems even when plotted versus reduced energy. In this context, it would be very important to elucidate whether proton-halo and neutron-halo systems actually behave differently.

With the purpose of providing further insight into these apparently controversial results for proton-halo systems, the respective data are revisited in the present work, putting special emphasis on potential weak points of the experimental methods that were mentioned above for each case. Section II presents some relevant details of the experiment with  ${}^{58}\text{Ni}$ . In Sec. III, the possible effect of bu protons on the data for  ${}^8\text{B} + {}^{58}\text{Ni}$  is investigated and correction factors are estimated. The absolute normalization of the data is discussed in Sec. IV. Section V reports an analysis of the compatibility of three different evaporation codes and discusses the most critical input parameters in each case. Possible model dependencies of the deduced fusion cross sections for both systems are explored by comparing the respective charged-particle multiplicities obtained with the different evaporation codes. The possible consistency of the two data sets is then reanalyzed within this context in Sec. VI. Finally, a summary and the conclusions of this work are presented in Sec. VII.

## II. THE ${}^8\text{B} + {}^{58}\text{Ni}$ EXPERIMENT

A complete description of the  ${}^8\text{B} + {}^{58}\text{Ni}$  experiment has been given in Ref. [1], but a few details relevant to the present work are discussed in more detail here. Secondary  ${}^8\text{B}$  beams with typical intensities of  $0.5\text{--}2.7 \times 10^4/\text{s}$  were used at the University of Notre Dame to bombard different Ni targets. To detect the protons emitted by the fused system, three or four  $\Delta E$ - $E$  silicon telescopes were used at backward angles, between  $105^\circ$  and  $158^\circ$ . Two additional telescopes (or single detectors) were placed at forward angles (usually  $\pm 45^\circ$ ) to monitor the beam. To compensate for the low beam rates, the experiment was performed in four stages and fairly thick natural Ni targets were used in some cases. Appropriate corrections were made to account for the presence of different Ni isotopes, whose validity was verified by comparing with equivalent measurements using an enriched  ${}^{58}\text{Ni}$  target at specific energies. The results were presented in Ref. [1] as a plot of  $\sigma_{\text{fus}}$  vs  $E_{\text{c.m.}}$ , but the respective proton cross sections  $\sigma_p$ , which are actually the purely experimental quantities, were not reported there mainly because of space limitations. They are reported in the present work in tabulated form in Sec. V A. In addition, a plot showing a typical angular distribution  $d\sigma_p/d\Omega$  is presented in Sec. III.

The thin  $\Delta E$  detectors of the backward telescopes were typically  $\sim 40 \mu\text{m}$  thick so low-energy protons could easily pass through them, but  $\alpha$  particles needed to surpass some threshold energy to be able to arrive at the thick  $E$  detector. Because of this, combined with the fact that many fewer  $\alpha$  particles than protons are emitted, only in a few cases could  $\alpha$  particles actually be detected and no complete analysis

of them was reported in Ref. [1]. In view of the suggested contamination of the proton yields discussed in the previous section, it was considered important in the present work to reanalyze that part of the data, putting special emphasis on doing a systematic evaluation of the observed  $\alpha$  particles. They could be detected only for the cases when rather thick natural Ni targets were used, i.e., at 18.9 MeV ( $5.6 \text{ mg/cm}^2$  tgt.) and 20.1, 22.1, and 23.8 MeV ( $2.22 \text{ mg/cm}^2$  tgt.). The results of this analysis are presented in Sec. V C. Further experimental details can be found in Ref. [1].

## III. BREAKUP PROTONS IN ${}^8\text{B} + {}^{58}\text{Ni}$

The proton angular distribution measured for the  ${}^8\text{B} + {}^{58}\text{Ni}$  system at  $E_{\text{c.m.}} = 23.7 \text{ MeV}$  [1] is displayed as the open circles in Fig. 1. As mentioned earlier, this corresponds to an inclusive measurement, i.e., all protons arriving at the detectors were measured regardless of how they were produced, whether by fusion-evaporation or breakup processes. Breakup measurements for this system were previously reported for a neighboring energy  $E_{\text{c.m.}} = 22.7 \text{ MeV}$  [10,11]. Detailed CDCC calculations by Tostevin *et al.* [4] reproduced the breakup data for both the angular distributions of the  ${}^7\text{Be}$  fragments and their energy distributions measured at several laboratory angles. It is thus realistic to expect that the corresponding predictions for breakup protons can be reliably used to estimate their contribution to the inclusive proton spectra. A bu-proton angular distribution extended to the angular range of interest in the present measurements became available recently [12] and is shown as the solid curve in Fig. 1. The respective contribution to the inclusive data amounts to about 5% and has been subtracted from the original data to obtain the solid circles in the figure. Compared to the

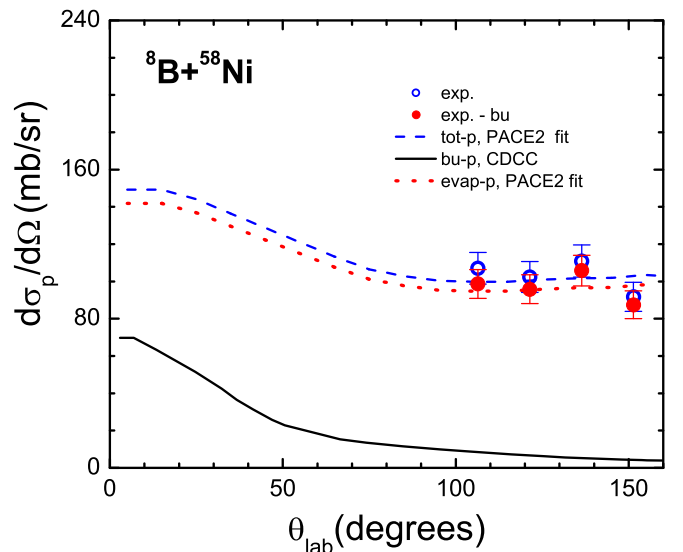


FIG. 1. Open circles, inclusive proton angular distribution measured at  $E_{\text{c.m.}} = 23.7 \text{ MeV}$  [1]; solid circles, data corrected for bu protons. The solid curve corresponds to a CDCC calculation of bu protons at  $E_{\text{c.m.}} = 22.7 \text{ MeV}$  [4,12], while the dashed (dotted) curve is a PACE2 fit to the open (solid) circles.

20% uncertainty reported in Ref. [1] for the corresponding  $\sigma_{\text{fus}}$  value, this 5% correction is relatively insignificant.

In addition to the breakup calculations shown in Fig. 1 (corresponding to  $E_{\text{lab}} = 25.8$  MeV), the energy spectra  $d\sigma_{\text{bu-p}}/dE_p(110^\circ\text{--}160^\circ)$  of breakup protons in the angular range of  $110^\circ$  to  $160^\circ$  were also calculated by Tostevin [12] for the three bombarding energies  $E_{\text{lab}} = 23, 25.8,$  and  $29.5$  MeV (see Fig. 6 in Ref. [5]). The energy integration of these spectra  $\int [d\sigma_{\text{bu-p}}/dE_p(110^\circ\text{--}160^\circ)]dE_p$  can be performed numerically, yielding values of 23.7, 24.0, and 20.1 mb, respectively. These numbers represent the total yields of bu protons for the given energies in the cited angular range. They can thus be compared with the solid angle integration of the experimental angular distributions,  $\int [d\sigma_{\text{exp}}/d\Omega]d\Omega$ , within the mentioned angular range, which would represent the total yields of inclusive (evaporation plus bu) protons within that range. In the case of the  $E_{\text{c.m.}} = 23.7$  MeV fusion measurement, for instance, the dashed curve in Fig. 1 was used, restricted to  $110^\circ \leq \theta \leq 160^\circ$ , to perform numerically the latter integration. Similar PACE2 fits to the measured proton cross sections for each experimental energy were used to obtain the solid angle integrations for the whole data set. Figure 2 illustrates the comparison of  $\int [d\sigma_{\text{exp}}/d\Omega]d\Omega$  versus  $\int [d\sigma_{\text{bu-p}}/dE_p(110^\circ\text{--}160^\circ)]dE_p$  as a function of the bombarding energy. Two important observations can be made: First, extrapolation of the low-energy trend of the CDCC calculations indicates that the lowest-energy experimental point may correspond mainly to bu protons; second, the contribution of bu protons to the rest of the experimental data will not move the points out of the reported uncertainty range after subtraction. The relative contribution of these protons, with respect to the absolute values of the experimental

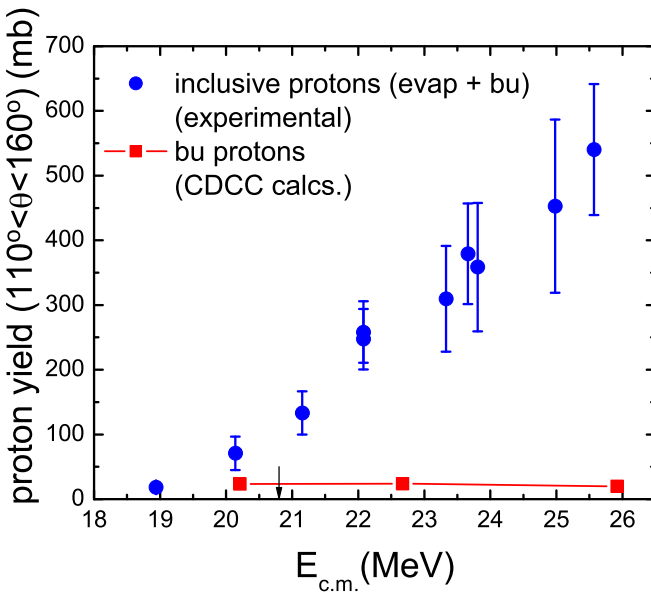


FIG. 2. Circles (squares) correspond to inclusive (bu) protons in the angular range  $110^\circ\text{--}160^\circ$ . The circles correspond to data of Ref. [1], while the squares were obtained from CDCC calculations [12] (see text). The vertical arrow indicates the position of the Coulomb barrier.

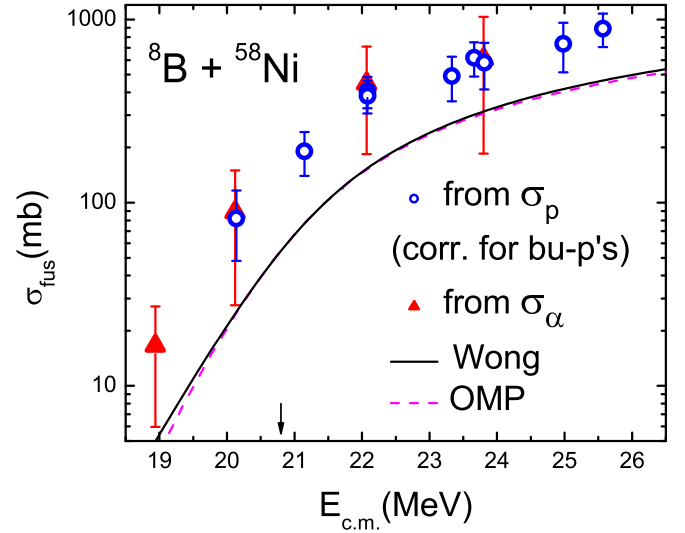


FIG. 3. Circles, fusion cross sections for  ${}^8\text{B} + {}^{58}\text{Ni}$  [1] after applying the corrections for bu protons as described in the text; triangles, the same, but obtained through evaporation  $\alpha$  particles (Sec. V C). The solid curve is the BPM prediction [13] for the barrier parameters of the bare potential:  $V_b = 20.8$  MeV,  $R_b = 8.9$  fm,  $\hbar\omega = 4.14$  MeV. The dashed curve was obtained from an optical model calculation using a short-range imaginary potential ( $W_0 = 50$  MeV,  $r_W = 1.06$  fm,  $a_W = 0.2$  fm).

data, becomes rapidly smaller for increasing energies and is insignificant above about  $E_{\text{c.m.}} = 22$  MeV.

It can be seen from Fig. 2 that the contribution of breakup protons is quite flat with energy, so a linear interpolation can be used to estimate corrections to the measurements for each experimental energy. The corrected fusion cross sections are presented as open circles in Fig. 3, where the lowest energy point measured in Ref. [1] has been discarded for the reasons explained earlier. The meaning of the triangles is described later in Sec. V C. The solid curve corresponds to a barrier penetration model (BPM) calculation with Wong's formula [13] using the barrier parameters of the bare potential, which was taken to be the São Paulo potential (SPP) [14]. The dashed curve is the result of an optical model calculation with a short-range imaginary potential ( $W_0 = 50$  MeV,  $r_W = 1.06$  fm,  $a_W = 0.2$  fm) which simulates an incoming-wave boundary condition, thus giving a realistic BPM prediction. The fact that the two curves in this figure do not show any significant difference from each other verifies that Wong's formula, in spite of the approximations involved [13], gives a reliable BPM result in the energy region of interest.

The above correction for bu protons relies on the overall accuracy of CDCC predictions of the type displayed with the solid curve in Fig. 1. The corresponding calculations assume that the  ${}^8\text{B}$  nucleus is formed by a  ${}^7\text{Be}$  core plus a valence proton, and the most important ingredients are the interaction potentials of core and valence proton with the target as well as that between the core and the valence proton. Calculations for three different combinations of these potentials, all of them quite reasonable, were done in Refs. [4,12]. In the angular region of interest ( $110^\circ\text{--}160^\circ$ ), the sensitivity of the results to

changes in these potentials indicates a maximum variation of  $\sim 38\%$  for  $d\sigma_p/d\Omega$  (see Fig. 5 in Ref. [5]). This maximum variation was actually taken as the relative uncertainty in the number of bu protons ( $N_{\text{bu-p}}$ ) and used all along the respective corrections; i.e., a relative uncertainty of 38% in  $N_{\text{bu-p}}$  has been folded in the respective error bars reported in Fig. 3. Although this is a fairly big uncertainty for  $d\sigma_p/d\Omega$ , its contribution to the global error bars in the corrected fusion cross sections is actually insignificant.

In summary, under the reasonable hypothesis that Tostevin's CDCC calculations [4,12] provide realistic bu estimations, it has been shown that the presence of breakup protons in the experimental data reported in Ref. [1] does not change the previous conclusion that a considerable fusion enhancement above the Coulomb barrier is present for the proton-halo system  ${}^8\text{B} + {}^{58}\text{Ni}$ .

#### IV. ABSOLUTE NORMALIZATION OF DATA

Absolute normalization of the data is an important issue, especially if one aims at making a point about fusion enhancement or suppression. It was mentioned in Ref. [1] that the reported fusion cross sections for  ${}^8\text{B} + {}^{58}\text{Ni}$  could be up to 10% higher or 5% smaller than the true values, but this should be reviewed on the basis of the discussion of Sec. III above. The absolute normalization factor is given by the product  $N_B \times N_{\text{tgt}}$ , where  $N_B$  ( $N_{\text{tgt}}$ ) is the number of  ${}^8\text{B}$  projectiles (target nuclei). This product was obtained from the “elastic” counts at two forward monitors (usually placed at the symmetric angles  $\theta = \pm 45^\circ$ ) by assuming Rutherford scattering. With small contributions from imprecisions in  $\theta$  and in the respective solid angles, the main uncertainty in  $N_B \times N_{\text{tgt}}$  is related precisely to the statistical uncertainty in the number of counts at the monitors. These could include some  ${}^7\text{Be}$  nuclei resulting from  ${}^8\text{B}$  bu, which are known to peak at forward angles and cannot be distinguished from  ${}^8\text{B}$ . An angular distribution for  ${}^7\text{Be}$  from bu reactions in  ${}^8\text{B} + {}^{58}\text{Ni}$  was reported in Refs. [10,11] for  $E_{\text{lab}} = 25.75$  MeV. Single-angle ( $\theta = \pm 45^\circ$ ) measurements for the additional energies of 25.0, 26.9, and 28.4 MeV have also been reported [15]. From these bu measurements, along with CDCC calculations [15–17], which describe the data well but also include predictions for lower energies, the respective contribution to the quasielastic ( ${}^8\text{B} + {}^7\text{Be}$ ) counts at the monitors can be estimated for each experimental energy in the  ${}^8\text{B} + {}^{58}\text{Ni}$  fusion measurements. This contribution, which varied from  $\sim 2.5\%$  for the higher energies to  $\sim 0.5\%$  for the lower energies, has been taken into account in obtaining the experimental data plotted in Fig. 3. It is interesting to note that correcting for the presence of  ${}^7\text{Be}$  nuclei at the monitors has the opposite effect on  $\sigma_{\text{fus}}$  as correcting for bu protons at the backward telescopes. Indeed, the former correction tends to increase the cross sections while the latter one tends to decrease them. At the highest energy, for instance, the 4% decrease in  $\sigma_{\text{fus}}$  owing to bu protons is counteracted by a 2.5% increase owing to  ${}^7\text{Be}$  nuclei at the monitors. At the lowest energies, the effect of bu protons dominates in this context. The overall uncertainties in the absolute normalization factors varied between 2% (for

the lowest energies) and 7% (for the highest energy) and these have been taken into account in the error bars shown in Fig. 3.

As for the  ${}^8\text{B} + {}^{28}\text{Si}$  data, there is not enough information given in Ref. [2] about the respective absolute normalization. In this case, a three-stage Si telescope (45, 45, 2000  $\mu\text{m}$ ) was used as an active target detector, which allowed for identification and partial counting of  $\alpha$  particles produced in fusion-evaporation reactions. Because thick Si targets were used and backward-going  $\alpha$  particles cannot be detected with this array, a suitable efficiency function is required to deduce differential-energy and integral-angle cross sections. An efficiency function of this type was deduced by the authors of Ref. [18], where essentially the same technique was applied to obtain inclusive  $\alpha$ -particle and proton measurements for the  ${}^{6,7}\text{Li} + {}^{28}\text{Si}$  systems. Monte Carlo calculations based on actual measurements of the corresponding energy and angular distributions were utilized, and an uncertainty of  $\sim 15\%$  was ascribed to the respective efficiency. The corresponding uncertainty in the case of the exotic  ${}^8\text{B}$  beam would probably be bigger and its actual value would have a direct impact on the uncertainty of the absolute normalization. In addition, the extraction of the fusion cross section from the thick-target yield required an extension of the measured data to lower energies. As described in Ref. [18], this necessitated a preliminary measurement at yet lower energy and a third-order polynomial fit. (See also Ref. [19], where an exponential extrapolation is instead applied to  ${}^7\text{Li} + {}^{28}\text{Si}$  data.) No information is given about the extrapolation used to estimate the lowest-energy  ${}^8\text{B} + {}^{28}\text{Si}$  cross section in Ref. [2].

It was emphasized in Ref. [18] that the thick-target technique is feasible specifically for reactions on silicon and only as long as both the angular distributions and the energy spectra of the reaction products are known from a separate experiment. For the case of the  ${}^8\text{B} + {}^{28}\text{Si}$  system there is no information given in Ref. [2] about data for the respective angular distributions and energy spectra. However, even if the  $\alpha$ -particle cross sections reported in the latter reference do not have additional uncertainties traceable to the efficiency function, which was not specified, an analysis of possible model dependency of the reported fusion cross sections is still important not only for  ${}^8\text{B} + {}^{28}\text{Si}$  but also for the  ${}^8\text{B} + {}^{58}\text{Ni}$  system. This is the subject of next section.

#### V. MAPPING $\sigma_{p,\alpha}$ INTO $\sigma_{\text{fus}}$ FOR ${}^8\text{B} + ({}^{58}\text{Ni}, {}^{28}\text{Si})$ , RESPECTIVELY: DISCUSSION OF EVAPORATION MODEL CALCULATIONS

Statistical-model calculations usually involve the selection of multiple sets of input parameters which may have a wide range of reasonable variation, sometimes leading to important sensitivity in the calculated results. There are in the literature several codes that can be used to perform this type of calculation. In an effort to estimate the model dependencies generated by use of a particular code, the results obtained with three different codes are compared in this section, with special emphasis on choosing appropriate input parameters to assess the compatibility of the corresponding physical calculations in each case. The aim is to establish an appropriate framework that permits a reliable comparison of the fusion results deduced

for the  ${}^8\text{B} + ({}^{28}\text{Si}, {}^{58}\text{Ni})$  systems through the use of these codes. As mentioned in Sec. I, the reported  $\sigma_{\text{fus}}$  values [1,2] were obtained by measuring different observables and using different statistical-model codes to deduce the fusion cross sections in each case. The codes that will be considered here are PACE2 [3], LILITA [20,21], and CASCADE [6,22]. [It is worth mentioning that two mistakes were discovered and corrected in the neutron optical-model potential parameters appearing in the PACE2 source code: (a) The coefficient of the  $E^2$  term in  $V$  was 0.0018, corrected to 0.00118 (see Refs. [23,24]). This was also corrected in LILITA; (b) the coefficient of the  $A^2$  term in  $r_D$  was  $4 \times 10^{-6}$ , corrected to  $2 \times 10^{-6}$ . The output results did not change significantly.]

### A. $\sigma_p \rightarrow \sigma_{\text{fus}}$ in ${}^8\text{B} + {}^{58}\text{Ni}$

The fusion cross sections reported in Ref. [1] for the  ${}^8\text{B} + {}^{58}\text{Ni}$  system were later reviewed [25] to investigate possible model dependency in the  $\sigma_p \rightarrow \sigma_{\text{fus}}$  mapping. The key quantities in this mapping, the proton multiplicities ( $M_p$ ), were initially calculated with PACE2 by using default values for the respective input parameters [1]. More specifically, the yrast line was always determined by the liquid-drop rotational energy, with the A. J. Sierk fission barrier assumed throughout the calculations, and the regular Wapstra mass table supplied with the code was used for all involved nuclei. The level density parameter was  $a = A/7.5$  (but the effect of variations in  $a$  was investigated). In addition, the experimental fusion cross sections  $\sigma_{\text{exp}}$  were used as an input (in an iterative way) because the code internally shifts the respective optical-model transmission coefficients to reproduce these values. It is important to remark, though, that the proton multiplicity,  $M_p$ , is not very sensitive to this. For instance, changing  $\sigma_{\text{exp}}$  by 30% would typically change  $M_p$  by only 1%.

The sensitivity of  $M_p$  to changes both in the involved level densities and in the relevant transmission coefficients was further investigated in Ref. [25]. It was argued there that the level-density parameter in the mass region of interest ( $60 \leq A \leq 70$ ) is better approximated by  $a = A/8.6$ , and the respective slope ( $1/8.6$ ) was varied within extreme limits. Also, calculations with the alternate code LILITA were performed. In PACE2, transmission coefficients  $T_l$  are calculated for the compound-nucleus values of  $A$  and  $Z$  and an extrapolation is made for subsequent decays by assuming that the respective  $T_l$  values are shifted in their kinetic energy dependence [26]. In contrast, LILITA explicitly calculates the necessary transmission coefficients [21]. The effects of both the sensitivity to changes in  $a$  and using an alternate code could be included in a global systematic uncertainty of  $\sim 7\%$  [25], which would not change the general conclusions stated in Ref. [1].

In the present work, new calculations with PACE2 and LILITA are performed, and in addition the code CASCADE is used to compute the relevant multiplicities. The CASCIP version [22] of the latter code, which treats isospin and parity exactly, was used here. As a first step, the mass tables used by the three codes were unified to the AME12 table [27]. As expected, this did not make any significant change in the respective output results. To further assess compatibility of CASCADE with PACE2 and LILITA, the following optical-model potential (OMP) param-

eters (which do not correspond to the default values in CASCADE) are used in a first calculation to get the respective transmission coefficients: For neutrons and protons, the parameters are taken from Perey and Perey [28], and for  $\alpha$  particles they are taken from Huizenga and Igo [29]. The three codes are essentially based on the Fermi gas formalism to describe level distributions, but different assumptions are used in each case to evaluate the actual densities. Possible differences in the proton multiplicity values owing to this reason can be ascribed to model dependency. To improve the accuracy of PACE2, which uses the Monte Carlo method, the source code was modified to be able to run with up to  $10^6$  events. This is the number of events used in all calculations reported here with PACE2 and LILITA (the latter code did not need modification to accomplish this).

Table I summarizes the  $M_p$  values obtained with each code for the  ${}^8\text{B} + {}^{58}\text{Ni}$  system, using always a level density parameter given by  $a = A/8.6$ . All the experimental energies of Ref. [1] are included and, for completeness, the fusion cross sections reported in Ref. [1] and the respective inclusive (evaporation + bu) proton cross sections are shown in columns 2 and 3, respectively. Notice that, while  $\sigma_{\text{fus}}^{(a)}$  depends on the  $M_p$  values used in Ref. [1],  $\sigma_p^{(b)}$  is a purely experimental quantity. It can be seen that the three codes give very similar results, although CASCADE predicts systematically lower values, which tends to increase the corresponding fusion cross sections. The  $\sigma_p$  values of column 4 include the corrections for bu protons discussed in Sec. III as well as those related to  ${}^7\text{Be}$  nuclei at the monitors, as discussed in Sec. IV. The line corresponding to the lowest energy was left blank because of the reasons explained in Sec. III. The mean  $M_p$  value for each energy (column 8), with an uncertainty estimated from the respective spread, was adopted to calculate the final  $\sigma_{\text{fus}}$  values (last column). As discussed in Ref. [1], it is safe to consider these as total fusion (TF) cross sections. Because the uncertainties in  $\langle M_p \rangle$  were already folded into the respective uncertainties in  $\sigma_{\text{fus}}$ , no additional systematic error persists. This is valid under the hypothesis that the values obtained for  $\langle M_p \rangle \pm \delta \langle M_p \rangle$  account properly for any model dependency. It is worth mentioning that the above  $\langle M_p \rangle$  values are systematically lower (by  $\sim 5\% - 8\%$ ) than the corresponding values that were originally used in Ref. [1] (the latter values were not included in Table I but could be easily obtained from columns 2 and 3:  $M_p = \sigma_p^{(b)}/\sigma_{\text{fus}}^{(a)}$ ). As a net effect, some of the final  $\sigma_{\text{fus}}$  values of Table I are actually slightly higher than the original values, as a comparison of columns 2 and 9 shows. The numbers given in column 9 of the table are the values that were actually plotted in Fig. 3. As discussed in connection with that figure, these new values of  $\sigma_{\text{fus}}$  which already account for bu protons are consistent (within uncertainties) with those reported in Ref. [1] (column 2). In particular, they do not change the conclusions therein about the presence of fusion enhancement for energies above the Coulomb barrier.

### B. $\sigma_\alpha \rightarrow \sigma_{\text{fus}}$ in ${}^8\text{B} + {}^{28}\text{Si}$

Using similar criteria, the above three codes were also used to calculate the  $\alpha$ -particle multiplicities,  $M_\alpha$ , required to make the mapping  $\sigma_\alpha \rightarrow \sigma_{\text{fus}}$  for the  ${}^8\text{B} + {}^{28}\text{Si}$  system. The respective  $\sigma_\alpha$  values were taken from Ref. [30], where

TABLE I. Previous fusion cross sections ( $\sigma_{\text{fus}}^{(a)}$ ) and inclusive and evaporation proton cross sections ( $\sigma_p^{(b,c)}$ ) for the  ${}^8\text{B} + {}^{58}\text{Ni}$  system. Respective  $M_p$  values obtained with the different codes, adopted  $\langle M_p \rangle$  values, and corresponding fusion cross sections obtained in the present work. The three codes used  $a = A/8.6$  and optical-model potential (OMP) parameters from Ref. [28] for  $n$  and  $p$  and from Ref. [29] for  $\alpha$  particles.

$E_{\text{c.m.}}$ (MeV)	$\sigma_{\text{fus}}^a$ Ref. [1] (mb)	$\sigma_p^b$ inclusive (mb)	$\sigma_p^c$ corrected (mb)	$M_p$ PACE2	$M_p$ LILITA	$M_p$ CASCADE	$\langle M_p \rangle$ adopted	$\sigma_{\text{fus}}$ final (mb)
18.9	$29 \pm 4$	$69 \pm 9$	—	2.32	2.23	2.14	$2.23 \pm 0.09$	—
20.1	$113 \pm 42$	$275 \pm 100$	$184 \pm 76$	2.34	2.25	2.13	$2.24 \pm 0.10$	$82 \pm 34$
21.1	$212 \pm 53$	$516 \pm 129$	$429 \pm 113$	2.34	2.27	2.12	$2.24 \pm 0.10$	$191 \pm 51$
22.1	$408 \pm 75$	$988 \pm 182$	$910 \pm 173$	2.33	2.28	2.12	$2.24 \pm 0.09$	$406 \pm 79$
22.1	$390 \pm 74$	$943 \pm 178$	$865 \pm 170$	2.34	2.28	2.12	$2.25 \pm 0.09$	$384 \pm 77$
23.3	$491 \pm 130$	$1197 \pm 316$	$1120 \pm 301$	2.34	2.38	2.13	$2.28 \pm 0.10$	$491 \pm 134$
23.7	$608 \pm 124$	$1476 \pm 302$	$1405 \pm 292$	2.33	2.35	2.13	$2.27 \pm 0.08$	$619 \pm 131$
23.8	$568 \pm 157$	$1385 \pm 383$	$1317 \pm 374$	2.34	2.33	2.14	$2.27 \pm 0.07$	$580 \pm 166$
25.0	$713 \pm 211$	$1740 \pm 515$	$1678 \pm 502$	2.34	2.37	2.14	$2.28 \pm 0.09$	$736 \pm 222$
25.6	$865 \pm 162$	$2103 \pm 394$	$2059 \pm 414$	2.32	2.42	2.18	$2.31 \pm 0.11$	$891 \pm 184$

<sup>a</sup>Data plotted in Fig. 2 of Ref. [1].

<sup>b</sup> $\sigma_{\text{fus}}^{(a)} = \sigma_p^{(b)}/M_p$  (for  $M_p$  see first paragraph of Sec. V A).

<sup>c</sup>Corrected for presence of  $bu$  particles at the detectors (Secs. III and IV).

an erratum to the original data of Ref. [2] was reported. The compound and residual nuclei in this case lie in the mass region  $23 \leq A \leq 36$ , where the level density parameter is better approximated by  $a = A/10.1$ . This conclusion stems from reviewing the published values of  $a$  for this mass range [31]. This expression for  $a$  was used in all three codes for calculations related to the present system. The results, including the deduced  $\sigma_{\text{fus}}$  values, are summarized in Table II. The  $\alpha$ -particle multiplicity values are plotted in Fig. 4. It can be seen that, except for one point, the Ref. [2] values are greater than any of the other calculations, especially at the lowest energy. This results in lower fusion cross sections at those energies. The reasons for this difference cannot be further studied because the parameters of the corresponding CASCADE calculations are not given in Ref. [2]. However, it is clear from this comparison that the  $M_\alpha$  values for this system are very sensitive to the parameters of the evaporation-model calculations, unlike the case of the  $M_p$  values for  ${}^8\text{B} + {}^{58}\text{Ni}$  discussed above.

The  $\sigma_{\text{fus}}$  values are plotted with squares in Fig. 5, along with those reported in Ref. [30] (open circles) for comparison. It can be seen that the two sets of values are consistent with each other within uncertainties. For the point corresponding to the lowest energy, however, the present analysis produces a

significantly larger fusion cross section. One should notice that the respective energy is about 4 MeV higher than the corresponding Coulomb barrier ( $V_b = 11.3$  MeV). Comparing with the BPM predictions for the SPP bare potential (solid curve), this lowest-energy point gives a hint of a possible enhancement above the barrier. This suggestion is further supported by the analysis of Sec. V D, but additional measurements for this system at lower energies would be needed to corroborate this hypothesis. The three higher energy points, however, do seem to present a fusion suppression as noted in Ref. [2].

### C. $\sigma_\alpha \rightarrow \sigma_{\text{fus}}$ in ${}^8\text{B} + {}^{58}\text{Ni}$

The experiment reported in Ref. [1] was optimized to measure protons from the  ${}^8\text{B} + {}^{58}\text{Ni}$  reaction, but some evaporation  $\alpha$  particles could also be seen in some situations. It was mentioned that the fusion cross sections deduced from the  $\alpha$  particle yields were consistent with those from the proton data, but no actual  $\alpha$ -particle data were presented in Ref. [1]. These data are reported here for the first time. The situations where  $\alpha$  particles could be detected correspond to cases where a rather thick target was used, which compensated for the low  $\alpha$ -particle cross-section values and for the fact that only a fraction of the  $\alpha$  particles could go through the  $\Delta E$

TABLE II.  $\alpha$ -particle cross sections ( $\sigma_\alpha$ ) [30] and multiplicity values ( $M_\alpha$ ) obtained for the  ${}^8\text{B} + {}^{28}\text{Si}$  system by using the codes PACE2, LILITA and CASCADE for  $a = A/10.1$ . OMP parameters were from Ref. [28] for  $n$  and  $p$  and from Ref. [29] for  $\alpha$  particles. The last column gives the deduced fusion cross sections.

$E_{\text{c.m.}}$ (MeV)	$\sigma_\alpha$ (mb)	$M_\alpha$ PACE2	$M_\alpha$ LILITA	$M_\alpha$ CASCADE	$\langle M_\alpha \rangle$ adopted	$\sigma_{\text{fus}}$ (mb)
15.6	$300 \pm 38$	0.462	0.380	0.439	$0.427 \pm 0.040$	$703 \pm 111$
19.4	$395 \pm 27$	0.570	0.483	0.554	$0.536 \pm 0.040$	$737 \pm 75$
23.3	$557 \pm 37$	0.686	0.599	0.667	$0.651 \pm 0.050$	$856 \pm 87$
27.2	$780 \pm 29$	0.816	0.698	0.759	$0.758 \pm 0.060$	$1029 \pm 90$

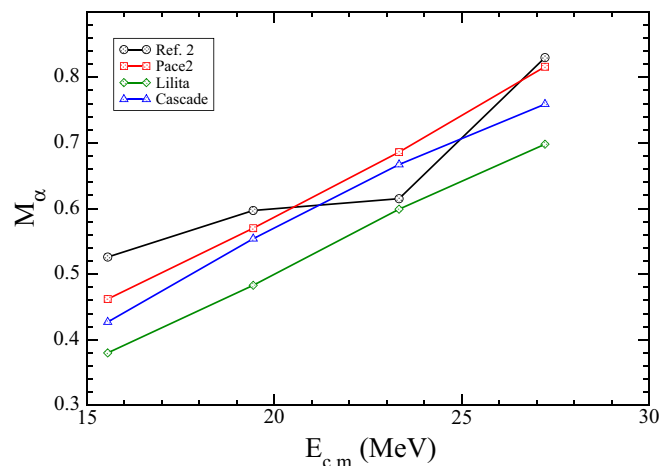


FIG. 4.  $\alpha$ -particle multiplicities for the  ${}^8\text{B} + {}^{28}\text{Si}$  system calculated with several different evaporation codes. The Ref. [2] values are calculated from the “ $R$  values” given in Ref. [30] using the formula  $M_\alpha = (R + 1)^{-1}$ .

detectors in the telescopes. Estimating these fractions from the known thicknesses of the  $\Delta E$  detectors and from the  $\alpha$ -particle energy spectra predicted by PACE2, an analysis similar to that summarized in Table II for the case of  ${}^8\text{B} + {}^{28}\text{Si}$  was made also for the present system. Fusion cross sections were thus obtained for four energies (Table III), which are illustrated with triangles in Fig. 3. These results show consistency with the  $\sigma_{\text{fus}}$  values obtained from the measured protons, albeit with very big error bars. An estimate of  $\sigma_{\text{fus}}$  for the lowest energy

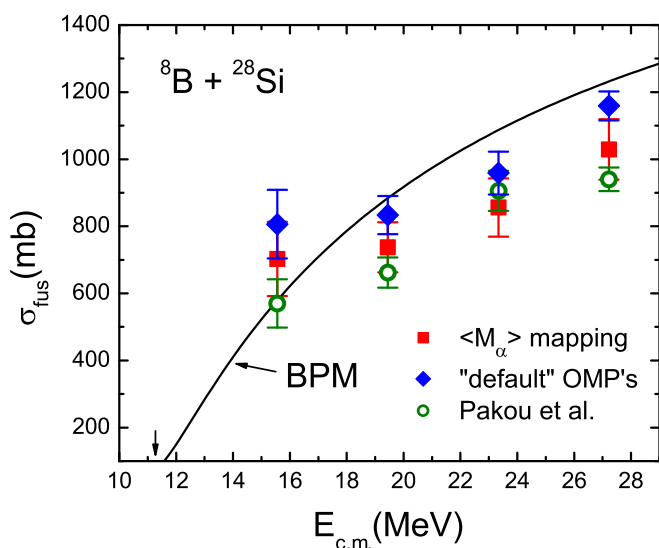


FIG. 5. Fusion cross sections for  ${}^8\text{B} + {}^{28}\text{Si}$  after applying the  $\sigma_\alpha \rightarrow \sigma_{\text{fus}}$  mapping summarized in Table II (squares). Diamonds correspond to an alternate mapping using the “recommended” optical-model parameters in CASCADE. For comparison, the  $\sigma_{\text{fus}}$  values originally reported [30] are also shown (circles). The solid curve is the BPM prediction for the barrier parameters of the bare (SPP) potential:  $V_b = 11.3$  MeV,  $R_b = 8.2$  fm,  $\hbar\omega = 3.38$  MeV.

TABLE III.  $\alpha$ -particle cross sections ( $\sigma_\alpha$ ) and multiplicity values ( $M_\alpha$ ) obtained for the  ${}^8\text{B} + {}^{58}\text{Ni}$  system by using the codes PACE2, LILITA, and CASCADE for  $a = A/8.6$ . OMP parameters were from Ref. [28] for  $n$  and  $p$  and from Ref. [29] for  $\alpha$  particles. The last column gives the deduced fusion cross sections. These data were taken during the experiment of Ref. [1] but had not been reported.

$E_{\text{c.m.}}$ (MeV)	$\sigma_\alpha$ (mb)	$M_\alpha$ PACE2	$M_\alpha$ LILITA	$M_\alpha$ CASCADE	$\langle M_\alpha \rangle$ adopted	$\sigma_{\text{fus}}$ (mb)
18.9	$5.3 \pm 2.6$	0.421	0.368	0.167	$0.319 \pm 0.127$	$17 \pm 11$
20.1	$31 \pm 17$	0.450	0.412	0.174	$0.345 \pm 0.138$	$89 \pm 61$
22.1	$174 \pm 70$	0.517	0.467	0.182	$0.389 \pm 0.168$	$447 \pm 263$
23.8	$260 \pm 135$	0.583	0.509	0.190	$0.427 \pm 0.197$	$609 \pm 424$

point, which had been discarded earlier on the basis of too much bu-proton contamination, could also be recovered.

#### D. Sensitivity to optical-model potentials

A test of the sensitivity of the calculated multiplicities to the involved transmission coefficients was made by doing CASCADE calculations for a different set of optical model parameters, i.e., those recommended by the author of this code. These parameters are taken from the following references: Becchetti and Greenlees [32] for protons, Rapaport [33] for neutrons, and Satchler [34] for  $\alpha$  particles. Compared to the  $M_p$  values reported for the  ${}^8\text{B} + {}^{58}\text{Ni}$  system in column 7 of Table I, the new values (not shown) are systematically higher but only by 3%–4%. Use of these new values to calculate  $\sigma_{\text{fus}}$  would not make any appreciable difference in Fig. 3; neither would it change the previous conclusion about fusion enhancement above the barrier for this system. As a matter of fact, these new  $M_p$  values fall safely within the uncertainties assigned to  $\langle M_p \rangle$  in Table I.

The situation is quite different for the case of the  ${}^8\text{B} + {}^{28}\text{Si}$  system. Although the respective  $M_p$  values of the new calculation also differ from the old ones by about 4%, the new  $M_\alpha$  values are systematically lower than those of column 5 in Table II, with differences of 11%–18%. These new values (not shown) fall out of the uncertainties assigned to  $\langle M_\alpha \rangle$  in Table II. The respective  $\sigma_{\text{fus}}$  values are considerably higher than those in the table, as illustrated by the diamonds in Fig. 5. With this alternate  $\sigma_\alpha \rightarrow \sigma_{\text{fus}}$  mapping, the lowest energy point, whose energy is  $\sim 4$  MeV above the barrier, does definitely show a fusion enhancement and only the two highest-energy points would be consistent with a possible (small) suppression.

In the case of the  $\alpha$ -particle measurements for  ${}^8\text{B} + {}^{58}\text{Ni}$ , summarized in Table III, the optical-model parameters used there give excellent agreement between the  $\sigma_{\text{fus}}$  values obtained in this table and those of Table I, corresponding to proton measurements, at all energies where both values were deduced. This should also be true for the lowest-energy triangle point shown in Fig. 3, where we do not have a corresponding proton measurement owing to possible contamination by bu protons.

## VI. COMPARISON OF REDUCED CROSS SECTIONS

For the purpose of comparing fusion data for different systems, we follow a prescription that has been widely used. In this approach, the barrier parameters  $V_b, R_b, \hbar\omega$  are obtained from a realistic bare potential and used to reduce the cross section and the energy through the expressions

$$\sigma_{\text{red}} = \frac{2E}{\hbar\omega R_b^2} \sigma, \quad E_{\text{red}} = \frac{E - V_b}{\hbar\omega}. \quad (1)$$

This prescription, based on the well-known analytic expression  $\sigma^W(E)$  derived for the cross section by Wong [13], had been used as early as 1996 by Prasad *et al.* [35] to compare a few systems with widely differing reactants, and was first applied to a systematic study of many systems by Gasques *et al.* [36] in 2004. More recently, it has been extensively studied by Canto *et al.* [7,8], mainly in the context of reactions with weakly bound projectiles. The detailed studies of the later authors have called new attention to this old prescription, bringing it into common use. If applied to  $\sigma^W(E)$ , one gets the so-called universal fusion function (UFF),

$$\sigma_{\text{red}}^W(E_{\text{red}}) = \frac{2E}{\hbar\omega R_b^2} \sigma^W(E) = \ln[1 + e^{(2\pi E_{\text{red}})}]. \quad (2)$$

In the present work, the double-folding SPP [14] was used to derive the barrier parameters, with default values for the matter and charge densities. These densities follow the systematics observed for many nuclei. With this procedure, any deviations from the reference curve [Eq. (2)] can, in principle, be ascribed either to static effects, related to deviations in the actual densities, or to dynamic effects, associated with some intrinsic properties of the involved nuclei. Possible deviations owing to inaccuracies in Wong's model can be monitored or discarded by comparing to OMP calculations such as the one represented by the dashed curve in Fig. 3. Because these inaccuracies occur mainly in the sub-barrier region, no OMP calculation is necessary for  ${}^8\text{B} + {}^{28}\text{Si}$  in Fig. 5.

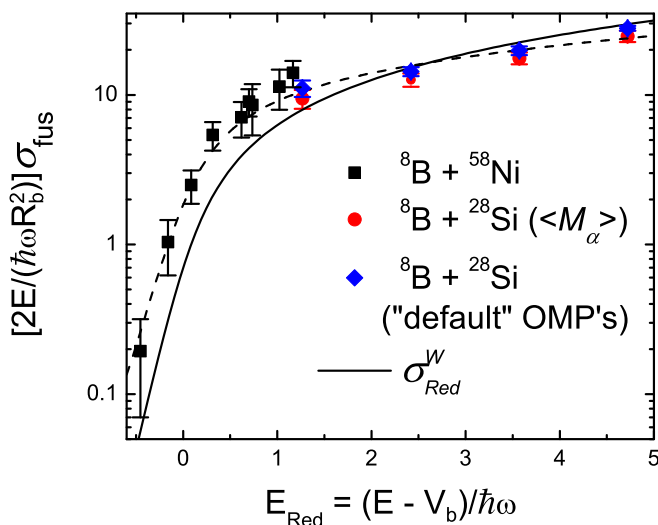


FIG. 6. Reduced fusion cross sections for  ${}^8\text{B} + ({}^{28}\text{Si}, {}^{58}\text{Ni})$ . The solid curve is the UFF and the dashed curve is to guide the eye.

Figure 6 shows a comparison of fusion data for the  ${}^8\text{B} + ({}^{28}\text{Si}, {}^{58}\text{Ni})$  systems, expressed in reduced units. For the heavier system, the  $\sigma_{\text{fus}}$  values of both Tables I and III have been used. In those cases where one or more points were at the same energy, they were replaced by the respective weighted mean and the appropriate error was calculated. In this plot, the lowest-energy point for the lighter system lies close in energy to the highest-energy point for the heavier system and, within uncertainties, they are consistent with each other independently of the mapping used to deduce  $\sigma_{\text{fus}}$ . One should notice that the points represented with diamonds, obtained for  ${}^8\text{B} + {}^{28}\text{Si}$  with the alternate  $\sigma_\alpha \rightarrow \sigma_{\text{fus}}$  mapping described in the previous section, do actually show a nice continuity with the points corresponding to  ${}^8\text{B} + {}^{58}\text{Ni}$ . While there seems to be no compelling argument to favor either one of the two mappings over the other, it is interesting to point out that the latter one tends to slightly lower  $\sigma_{\text{fus}}({}^8\text{B} + {}^{58}\text{Ni})$  while increasing  $\sigma_{\text{fus}}({}^8\text{B} + {}^{28}\text{Si})$ . Therefore, this alternate mapping would bring the data sets for both systems into even better consistency with each other, within the framework of the reduced plot of Fig. 6. The dashed curve in this figure depicts the trend of the reduced data. It indicates a fusion enhancement up to at least  $E_{\text{red}} = 1.5$ , i.e., at energies about 1.5 units of  $\hbar\omega$  above the barrier. For  $E_{\text{red}} = 1$ , corresponding to 4.1 MeV above the barrier for  ${}^8\text{B} + {}^{58}\text{Ni}$ , the enhancement factor would be  $\sim 1.5$ . Altogether, these results are consistent with the presence of fusion enhancement above the Coulomb barrier energy for both  ${}^8\text{B}$  systems.

## VII. SUMMARY AND CONCLUSIONS

The fusion cross sections reported previously for the proton-halo systems  ${}^8\text{B} + ({}^{58}\text{Ni}, {}^{28}\text{Si})$  [1,2] were revisited. The corrections for  $\alpha$  particles in the case of  ${}^8\text{B} + {}^{58}\text{Ni}$  were found to be small except at the lowest energy. Discarding this lowest-energy point, the respective corrections did not move the reported cross sections out of the uncertainties given in Ref. [1]. In particular, the conclusion concerning the existence of fusion enhancement above the barrier remains valid even after a detailed analysis of model dependency. This analysis was carried out using three statistical-model codes with reasonable input data. In the case of the  ${}^8\text{B} + {}^{28}\text{Si}$  system, where  $\alpha$  particles were measured instead of protons, a similar study with the same codes showed a higher degree of model dependency. The fact that the respective  $\alpha$ -particle multiplicities are small in comparison with those corresponding to protons makes the results of the calculations less stable in this case. Within the uncertainties that take this model dependency into account, the deduced fusion cross section data for both systems are consistent with each other at the single point where they overlap when viewed in a reduced plot.

Coupled-channel calculations for the  ${}^8\text{B} + {}^{58}\text{Ni}$  system [5] have discarded target excitations as the source of the fusion enhancement in this case. Using semiclassical arguments, it was speculated in Ref. [37] that some process similar to Coulomb polarization might be behind the observed enhancement. Within a time-dependent quantum mechanical approach, it has been shown [38,39] that the fusion probability should be

enhanced by the presence of the halo nucleon for proton-halo nuclei and suppressed for neutron-halo nuclei. Both complete and incomplete fusion were included in this calculation. A gradual process of Coulomb polarization, eventually leading to breakup, was proposed as the mechanism explaining the fusion enhancement. A similar conclusion was reached in Ref. [40], where a simple model was used to describe the dynamical effects of break-up processes in the sub-barrier fusion of weakly bound nuclei. However, additional theoretical work is needed to achieve a better understanding of the observed

fusion enhancement below and just above the barrier for the proton-halo system  ${}^8\text{B} + {}^{58}\text{Ni}$ .

### ACKNOWLEDGMENTS

This work has been partially supported by CONACYT (México), and by the US National Science Foundation under Grants No. PHY09-69456, No. PHY-0969058, and No. PHY14-01343.

- 
- [1] E. F. Aguilera *et al.*, *Phys. Rev. Lett.* **107**, 092701 (2011).  
 [2] A. Pakou *et al.*, *Phys. Rev. C* **87**, 014619 (2013).  
 [3] A. Gavron, *Phys. Rev. C* **21**, 230 (1980).  
 [4] J. A. Tostevin, F. M. Nunes, and I. J. Thompson, *Phys. Rev. C* **63**, 024617 (2001).  
 [5] J. Rangel, J. Lubian, P. R. S. Gomes, B. V. Carlson, L. C. Chamon, and A. Gómez-Camacho, *Eur. Phys. J. A* **49**, 57 (2013).  
 [6] F. Pühlhofer, *Nucl. Phys. A* **280**, 267 (1977).  
 [7] L. F. Canto, P. R. S. Gomes, J. Lubian, L. C. Chamon, and E. Crema, *J. Phys. G: Nucl. Part. Phys.* **36**, 015109 (2009).  
 [8] L. F. Canto, P. R. S. Gomes, J. Lubian, L. C. Chamon, and E. Crema, *Nucl. Phys. A* **821**, 51 (2009).  
 [9] J. J. Kolata and E. F. Aguilera, *Phys. Rev. C* **79**, 027603 (2009).  
 [10] V. Guimarães, J. J. Kolata, D. Peterson, P. Santi, R. H. White-Stevens, S. M. Vincent, F. D. Becchetti, M. Y. Lee, T. W. O'Donnell, D. A. Roberts, and J. A. Zimmerman, *Phys. Rev. Lett.* **84**, 1862 (2000).  
 [11] J. J. Kolata, V. Guimarães, D. Peterson, P. Santi, R. H. White-Stevens, S. M. Vincent, F. D. Becchetti, M. Y. Lee, T. W. O'Donnell, D. A. Roberts, and J. A. Zimmerman, *Phys. Rev. C* **63**, 024616 (2001).  
 [12] J. A. Tostevin, cited as "private communication" in Ref. [5].  
 [13] C. Y. Wong, *Phys. Rev. Lett.* **31**, 766 (1973).  
 [14] L. C. Chamon, B. V. Carlson, L. R. Gasques, D. Pereira, C. De Conti, M. A. G. Alvarez, M. S. Hussein, M. A. Cândido Ribeiro, E. S. Rossi, Jr., and C. P. Silva, *Phys. Rev. C* **66**, 014610 (2002).  
 [15] E. F. Aguilera, E. Martínez-Quiroz, T. L. Belyaeva, J. J. Kolata, and R. Leyte-Gonzalez, *Phys. Atom. Nucl.* **71**, 1163 (2008).  
 [16] T. L. Belyaeva, E. F. Aguilera, E. Martínez-Quiroz, A. M. Moro, and J. J. Kolata, *Phys. Rev. C* **80**, 064617 (2009).  
 [17] T. L. Belyaeva, P. Amador-Valenzuela, E. F. Aguilera, E. Martínez-Quiroz, and J. J. Kolata, *Eur. Phys. J. Web Conf.* **66**, 3008 (2014).  
 [18] A. Pakou, A. Musumarra, D. Pierrousakou, N. Alamanos, P. A. Assimakopoulos, N. Divis, G. Doukelis, A. Gillibert, S. Harissopoulos, G. Kalyva, M. Kokkoris, A. Lagoyannis, T. J. Mertzimekis, N. G. Nicolis, C. Papachristodoulou, G. Perdikakis, D. Roubos, K. Rusek, S. Spyrou, and Ch. Zarkadas, *Nucl. Phys. A* **784**, 13 (2007).  
 [19] A. Musumarra, P. Figuera, F. DeLuca, A. DiPietro, P. Finocchiaro, M. Fisichella, M. Lattuada, A. Pakou, M. G. Pellegriti, G. Randisi, G. Scalia, C. Scirè, S. Scirè, V. Scuderi, D. Torresi, and M. Zadro, *Nucl. Inst. Methods Phys. Res.* **A612**, 399 (2010).  
 [20] J. Gomez del Campo and R. G. Stokstad, ORNL Report TM-7295, 1981.  
 [21] J. Gomez del Campo (private communication).  
 [22] M. N. Harakeh, D. H. Dowell, G. Feldman, E. F. Garman, R. Loveman, J. L. Osborne, and K. A. Snover, *Phys. Lett. B* **176**, 297 (1986).  
 [23] D. Wilmore and P. E. Hodgson, *Nucl. Phys.* **55**, 673 (1964).  
 [24] P. Marmier and E. Sheldon, *Physics of Nuclei and Particles* (Academic Press, San Diego, 1970), Vol. 2, p. 1107.  
 [25] P. Amador-Valenzuela, E. F. Aguilera, E. Martínez-Quiroz, D. Lizcano, T. L. Belyaeva, and J. J. Kolata, *J. Phys.: Conf. Ser.* **492**, 012003 (2014).  
 [26] A. Gavron, in *Computational Nuclear Physics 2: Nuclear Reactions*, edited by K. Langanke, J. A. Maruhn, and S. E. Koonin (Springer, New York, 1993), p. 108.  
 [27] M. Wang, G. Audi, A. H. Wapstra, F. G. Kondev, M. MacCormick, X. Xu, and B. Pfeiffer, *Chinese Phys. C* **36**, 1603 (2012).  
 [28] C. M. Perey and F. G. Perey, *At. Data Nucl. Data Tables* **17**, 1 (1976).  
 [29] J. R. Huizenga and G. Igo, *Nucl. Phys.* **29**, 462 (1962).  
 [30] A. Pakou *et al.*, *Phys. Rev. C* **87**, 049901(E) (2013).  
 [31] R. G. Stokstad, in *Treatise on Heavy-Ion Science*, edited by D. A. Bromley (Plenum Press, New York, 1985), Vol. 3, p. 83.  
 [32] F. D. Becchetti, Jr., and G. W. Greenlees, *Phys. Rev.* **182**, 1190 (1969).  
 [33] J. Rapaport, V. Kulkarni, and R. W. Finlay, *Nucl. Phys. A* **330**, 15 (1979).  
 [34] G. R. Satchler, *Nucl. Phys.* **70**, 177 (1965).  
 [35] N. V. S. V. Prasad, A. M. Vinodkumar, A. K. Sinha, K. M. Varier, D. L. Sastry, N. Madhavan, P. Sugathan, D. O. Kataria, and J. J. Das, *Nucl. Phys. A* **603**, 176 (1996).  
 [36] L. R. Gasques, L. C. Chamon, D. Pereira, M. A. G. Alvarez, E. S. Rossi, Jr., C. P. Silva, and B. V. Carlson, *Phys. Rev. C* **69**, 034603 (2004).  
 [37] E. F. Aguilera, E. Martínez-Quiroz, P. Amador-Valenzuela, A. Gómez-Camacho, and J. J. Kolata, *J. Phys.: Conf. Ser.* **492**, 012002 (2014).  
 [38] T. Nakatsukasa, K. Yabana, M. Ito, M. Kobayashi, and M. Ueda, *Prog. Theor. Phys. Suppl.* **154**, 85 (2004).  
 [39] M. Ito, K. Yabana, T. Nakatsukasa, and M. Ueda, *Nucl. Phys. A* **787**, 267 (2007).  
 [40] R. Kumar, J. A. Lay, and A. Vitturi, *Phys. Rev. C* **89**, 027601 (2014).